Formation of olivine veins by reactive fluid flow in a dehydrating serpentinite

K. Huber[1], **J.C. Vrijmoed**[1], **T. John**[1]

[1]Freie Universität Berlin, Malteserstraße 74-100, 12247 Berlin, Germany

Key Points:

- brucite abundant domains release a fluid with a lower silica content than antigorite-rich domains
- reactive fluid flow can trigger dehydration
- preexisting vein-like structures form pathways for a low silica fluid to generate near pure olivine veins

Corresponding author: Konstantin Huber, konstantin.huber@fu-berlin.de

Abstract

Many exposed high-pressure meta-serpentinites comprise a channelized network of olivine-rich veins which formed during dehydration at depth and served as pathway for fluid escape. Previous studies showed that the formation of an olivine enriched vein-like interconnected porosity network on the μm-scale is controlled by chemical heterogeneities in the rock. However, the evolution towards larger scale and nearly pure olivine veins is not yet well understood. Here we study the effects of reactive fluid flow on a developing vein system during dehydration. We use thermodynamic equilibrium calculations to investigate the effects of bulk silica content variations in serpentinites on the dehydration reaction of antigorite + brucite = olivine + free fluid and silica content of this fluid phase. We develop a numerical model combining the effects of intrinsic chemical heterogeneities with reactive silica transport. Increasing temperatures lead to local fluid overpressure and the liberation of a silica-poor fluid in a subdomain with initially increased bulk iron and decreased silica content. The fluid overpressure drives fluid flow into other subdomains where the fluid enhances dehydration and leads to olivine enrichment in an iron-enriched vein. Our model shows how reactive silica transport can lead to vein widening and olivine enrichment within the veins as observed in the Erro Tobbio meta-serpentinites. Thus, reactive fluid flow is a critical step in the evolution towards a larger scale vein system and a dynamic porosity evolution by accounting for a chemical feedback between the dehydrating rock and the liberated fluid.

1 Introduction

Serpentinites represent the major fluid source within subducting oceanic plates and carry large amounts of water stored in hydrous minerals into subduction zones worldwide (Scambelluri et al., 1995; van Keken et al., 2011; Rüpke et al., 2004). Fully hydrated oceanic mantle can store up to 13 wt. % water that is released in a series of dehydration reactions (Ulmer & Trommsdorff, 1995; Rüpke et al., 2004; Plümper et al., 2017). These fluids have large effects on important geodynamic processes such as earthquakes (Moreno et al., 2014; Jung et al., 2004; Hacker et al., 2003) and arc magmatism (Mazza et al., 2020; John et al., 2012; Schmidt & Poli, 1998)

Dehydration reactions lead to densification of the slab constituting solid and therefore the formation of a fluid-filled porosity. The first porosity forms on the sub-mm-scale heterogeneously distributed in the rock (fig. 1a), as defined by the local bulk composition (Plümper et al., 2017). As dehydration continues, these first vein-like porosity structures connect and form a vein network (1b) that allows fluid flow in the rock. Finally, the fluid escapes (1c) by the formation of either fracture-like (e.g. Padrón-Navarta et al., 2010; Herms et al., 2012; Spandler et al., 2011; John et al., 2008) or porosity wave-like fluid pathways (Miller et al., 2003; Skarbek & Rempel, 2016; Chen et al., 2019; Piccoli et al., 2021).

One of the key dehydration reactions in hydrated slab mantle is the breakdown of brucite and antigorite to form olivine and an aqueous fluid phase (Ulmer & Trommsdorff, 1995). In partially dehydrated serpentinites the occurrence of metamorphic olivine after serpentine is used as indicator that these domains underwent dehydration. Such olivine-rich dehydration structures are commonly observed in formerly subducted high-pressure ophiolites, e.g. the Cerro del Almirez massif in Spain (López Sánchez-Vizcaíno et al., 2005, 2009), in the Sanbagwa metamorphic belt in Japan (Fukumura et al., 2019) or in various locations in the Western Alps (Groppo & Compagnoni, 2007; Scambelluri et al., 1991; Clément et al., 2020; Kempf et al., 2020). In many cases olivine enrichment in these rocks is associated with deformation structures such as mylonitic shear zones (Hermann et al., 2000) or pseudotachylites (Magott et al., 2020), but occasionally these rocks also contain an olivine-rich vein network in parts with only very little deformation. A key locality to study these olivine-rich veins are the meta-serpentinites of the Erro Tobbio unit

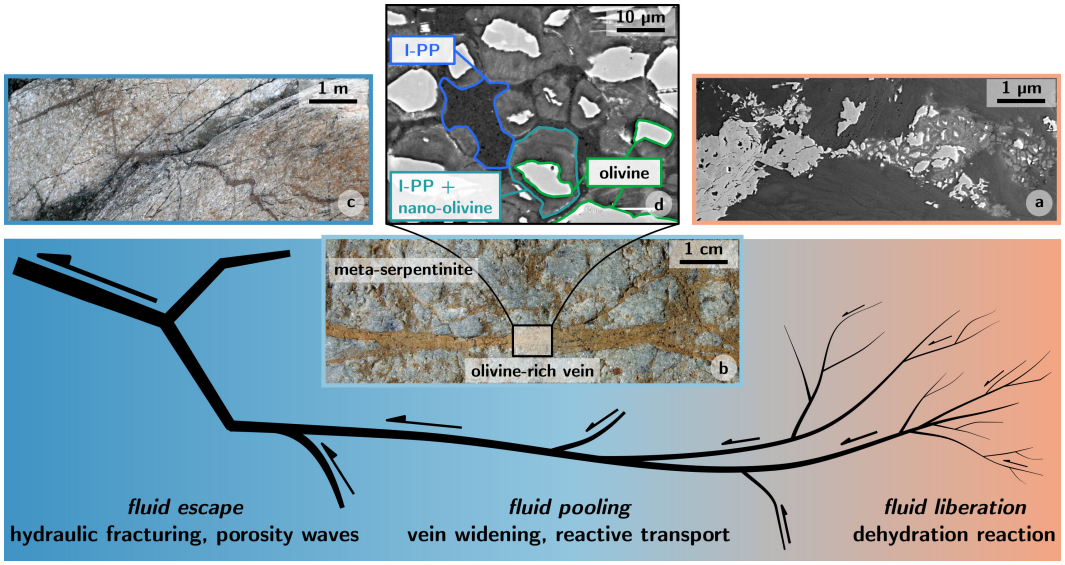

Figure 1. Channelized network of dehydration-related olivine-rich veins as observed in the Erro-Tobbio meta-serpentinites. Colors indicate the three main stages of rock dehydration on different length scales. The dominant processes acting on each scale are listed at the bottom. Arrows indicate the direction and magnitude of fluid flow in the veins. Figures a)-c) show the natural occurrence of olivine-rich veins on the μm-, the cm- and the m-scale, respectively. d) shows the mineral assemblage in an olivine-rich vein, displaying the reaction of intermediate phyllosilicate-phase (I-PP, Plümper et al. (2017)) to metamorphic olivine.

in the Ligurian Alps in Italy (Scambelluri et al., 1995, 1991; Plümper et al., 2017). These rocks show both olivine-rich mylonites and the olivine-rich vein network in an undeformed body of antigorite-rich country rock (fig. 1b and c).

Plümper et al. (2017) showed that intrinsic local variations in the bulk rock chemistry cause the formation of vein-like porosity structures on the sub-mm-scale that are enriched in olivine compared to the antigorite-rich surrounding matrix (fig. 1a). This suggests that dehydration is leading to fluid channeling directly at the onset of the dehydration process. On the base of measured variations in Vp/Vs ratios such a dynamic vein-network formation, which eventually results in fluid release from the dehydrating rock volume, has also been suggested in a seismological study of the slab mantle of the descending Nazca plate beneath Chile (Bloch et al., 2018). And in fact, magnetotelluric data derived from the Cascadia subduction zone imply that fluid flow from the slab is highly focused and directly feeds the arc volcanoes (McGary et al., 2014). Although such large-scale fluid flow focusing has been recently studied in numerical models (e.g. Wilson et al., 2014; Cerpa et al., 2017), these large-scale models do not provide a conceptual view on how the fluid flow mechanisms operate on the small scale and which mechanisms control and define the transition towards outcrop and even plate scales. Accordingly, a key question remains how small-scale dehydrating systems as described by Plümper et al. (2017) then further develop into a near-pure olivine vein network that occurs on the outcrop (fig. 1, Scambelluri et al. (1995)) and thus likely even larger scales. This step is needed to derive a mechanistic understanding on how small-scale veins organize themselves on the larger scale to eventually form efficient fluid escape pathways that are able to drain the descending slab.

So far, the effects of deformation and the importance of chemical heterogeneities have been addressed in various studies. These studies often do not consider the effects of reactive transport on the evolution of the dehydration vein network. Plümper et al. (2017) for example treated the liberated fluid as pure H_2O and have not explored the chemistry of the liberated fluid and its interaction with the wall rock system. However, changes in the fluid chemistry certainly feedback into the chemistry of the affected rock volume may thus drive mineral reactions which consequently result in dehydration and accordingly a change in the mineral assemblage.

Here we study the effects of reactive fluid flow on the development of the dehydration vein network in an undeformed serpentinite during dehydration of a subducting slab. Our model is used to show how changes in the silica content of the fluid can lead to enhanced dehydration, vein widening, and olivine purification within the vein.

2 Model Concept

2.1 Equations and Solution Strategy

Our model is described by three balance laws for total mass (1), total silica mass (2) and nonvolatile mass (3), i.e. a chemical component that is not dissolved in the fluid phase. The formulation of the reactive transport model follows the approach also used by Beinlich et al. (2020). By substituting Darcy's law to describe fluid flow in the porous medium, negecting solid velocity divergence ($\nabla \cdot v_s = 0$) and integrating over the nonvolatile mass balance, these balance laws can be expressed in the form of equations 1-3.

$$\frac{\partial \left(\rho_s \left(1-\phi\right)+\rho_f \phi\right)}{\partial t} = \nabla \cdot \left(\rho_f \frac{k_0 \phi^3}{\mu} \nabla P_f\right) \tag{1}$$

$$\frac{\partial \left(\rho_s c_s \left(1-\phi\right)+\rho_f c_f \phi\right)}{\partial t} = \nabla \cdot \left(\rho_f c_f \frac{k_0 \phi^3}{\mu} \nabla P_f + \rho_f c_f \phi D_c \nabla c_f\right) \tag{2}$$

$$\phi = 1 - \frac{\rho_s^0 \left(1-c_s^0-X_h^0\right)\left(1-\phi^0\right)}{\rho_s \left(1-c_s-X_h\right)} \tag{3}$$

In total, these three equations contain seven unknowns (P_f, ϕ, c_f, c_s, ρ_s, ρ_f, X_h). Three of these variables (P_f, c_f and ϕ) are obtained by solving the equations 1-3 by using a finite difference code implemented in MATLAB. The remaining four unknowns have been precomputed and stored in lookup tables from where they can be interpolated using the assumption of local equilibrium (Malvoisin et al., 2015; Plümper et al., 2017). To combine the findings of Plümper et al. (2017) with the effects of reactive transport (Beinlich et al., 2020), we formulate a 2D model with a vein placed in a chemically distinct matrix, representing a vein-like heterogeneity as shown in fig. 1b) that is then subject to reactive fluid flow.

2.2 Equilibrium Thermodynamics

To close the set of equations for the remaining four unknowns, we used Gibbs minimization (Vrijmoed & Podladchikov, 2015) to calculate phase diagrams for 75 different bulk compositions with varying bulk silica and bulk iron contents in the range of 0.1-2.0 GPa and 100-550 °C. From these phase diagrams we postprocessed the values for the thermodynamic closure relationships (ρ_s, ρ_f, c_s, X_h) and expressed them as functions of fluid pressure (P_f), fluid composition (c_f) and iron content for a fixed temperature (T). Once the values for P_f and c_f are obtained from equation (1) and (2), respectively, the closure relationships can be interpolated from the precomputed equilibrium data.

All thermodynamic calculations were performed in the FeO-MgO-SiO_2-H_2O (FMSH) system. The bulk compositions consist of Fe-poor and Fe-rich antigorite to which silica is added to cover a full range of compositions spanning a suitable range of fluid compositions. The initial bulk compositions used in each of the three domains of our model are

Table 1. Notation used in our model

Symbol	Meaning	Unit
ρ_s	solid density	$\mathrm{kg\,m^{-3}}$
ρ_s^0	initial solid density at T_0	$\mathrm{kg\,m^{-3}}$
ρ_f	fluid density	$\mathrm{kg\,m^{-3}}$
ϕ	porosity	volume fraction
ϕ^0	initial porosity at T_0	volume fraction
c_f	SiO_2 content of fluid	weight fraction
c_s	SiO_2 content of solid	weight fraction
c_s^0	initial SiO_2 content of solid at T_0	weight fraction
X_h	H_2O content of solid	weight fraction
X_h^0	initial H_2O content of solid at T_0	weight fraction
P_f	fluid pressure	GPa
P_f^0	initial fluid pressure	GPa
D_c	diffusion constant	$\mathrm{m^2\,s^{-1}}$
k_0	permeability	$\mathrm{m^2}$
μ	dynamic viscosity	$\mathrm{m^2\,s^{-1}}$
T	temperature	°C

shown in table 3. In our model we considered as solid phases antigorite, brucite, olivine, orthopyroxene, talc and quartz and a SiO_2-H_2O fluid phase. To account for the formation of Fe-Mg solid solutions in minerals and for SiO_2-H_2O mixing in the fluid we used the solution models given in table 2.

Table 2. Solution models used for the phase diagram calculations

Phase	Solution model used
Antigorite	Padrón-Navarta et al. (2013)
Olivine	T. J. B. Holland and Powell (1998)
Orthopyroxene	Powell and Holland (1999)
Talc	T. J. B. Holland and Powell (1998)
Brucite	Ideal
Fluid	Ideal mixing with a combination of CORK EOS for H_2O (T. Holland & Powell, 1991) with aqueous silica neutral species from (T. J. B. Holland & Powell, 1998)

3 Results

3.1 Effect of Iron on the Onset of Dehydration

The local bulk composition controls the stability and the abundance of hydrous minerals and thus the onset of dehydration (e.g. Plümper et al., 2017). Iron is one of the components with a strong influence on the temperature at which the first dehydration reaction occurs (e.g., Merkulova et al., 2016; Spear, 1993). A high iron content decreases the temperature at which the first dehydration reaction occurs by stabilizing brucite and iron-rich antigorite at lower temperatures. This effect can be seen in figure 2 showing pseudosection diagrams for two serpentinite bulk compositions that are varied only in their iron content. In the iron rich system (a) the onset of dehydration, shown by the

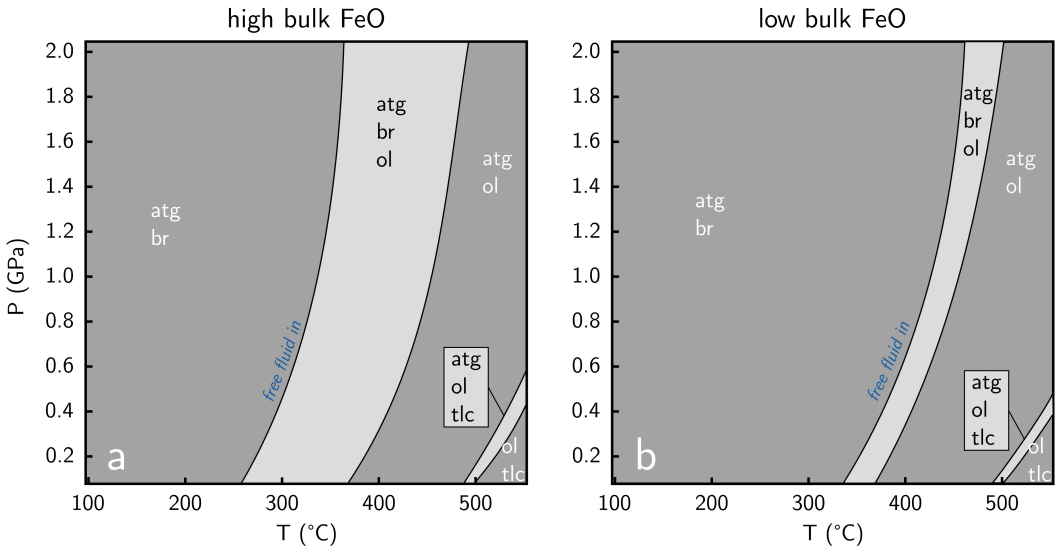

Figure 2. P-T diagrams for two typical serpentinite bulk compositions with identical silica and varying iron contents. A higher iron content (a) lowers the temperature for the onset of dehydration (marked by the 'free fluid in' reaction line) by ca. 100 °C compared to the iron-poor composition (b). atg = antigorite, br = brucite, ol = olivine, tlc = talc. Different grey shadings represent varying degrees of freedom with respect to the Gibbs phase rule.

reaction line labeled 'free fluid in', is lowered by 100 °C compared to the iron-poor system (b).

However, because of its very low solubility at deep subduction zone conditions, iron has only a minor effect on the composition of the liberated fluid (Manning, 2004; Charlou et al., 2002; Ding & Seyfried, 1992). Silica on the other hand is abundant in serpentinites and has a significantly higher solubility (Manning, 2004). Therefore, in order to study first-order mechanisms of reactive transport in serpentinites, we investigate the effect of silica as the metasomatic agent in our model.

3.2 Effect of Bulk Silica Variation on Dehydration

If silica can be either stored in the solid or be dissolved in the fluid phase, the equilibrium composition of both phases depends on the bulk composition of the entire system and especially on the total silica abundance. To study the effects that varying bulk silica contents have on a dehydrating serpentinite, we calculated pseudosection diagrams for two serpentinite bulk compositions with identical bulk iron but varying bulk silica contents. From these pseudosection diagrams we postprocessed the equilibrium thermodynamic parameters of interest, especially the lookup tables. Figure 4 shows results of those calculcations that demonstrate the effect of bulk silica variations on dehydration with increasing P-T conditions. The left and right columns show the results for the low silica and the high silica system, respectively. The range of P-T conditions captures the dehydration reaction of antigorite and brucite to form olivine and a free fluid. In the low silica system dehydration starts at lower temperatures than in the higher SiO_2 system (fig. 3a and b). Consequently, nearly 90 vol. % olivine forms, whereas in the higher bulk SiO_2 system the olivine abundance increases only slightly (fig. 3c and d). The reason for this is that a low silica content stabilizes more brucite which is only stable up to temperatures of 450 °C and 475 °C in the low and the high bulk silica system, respectively. As brucite contains large amounts of H_2O, the strong decrease in the brucite content also

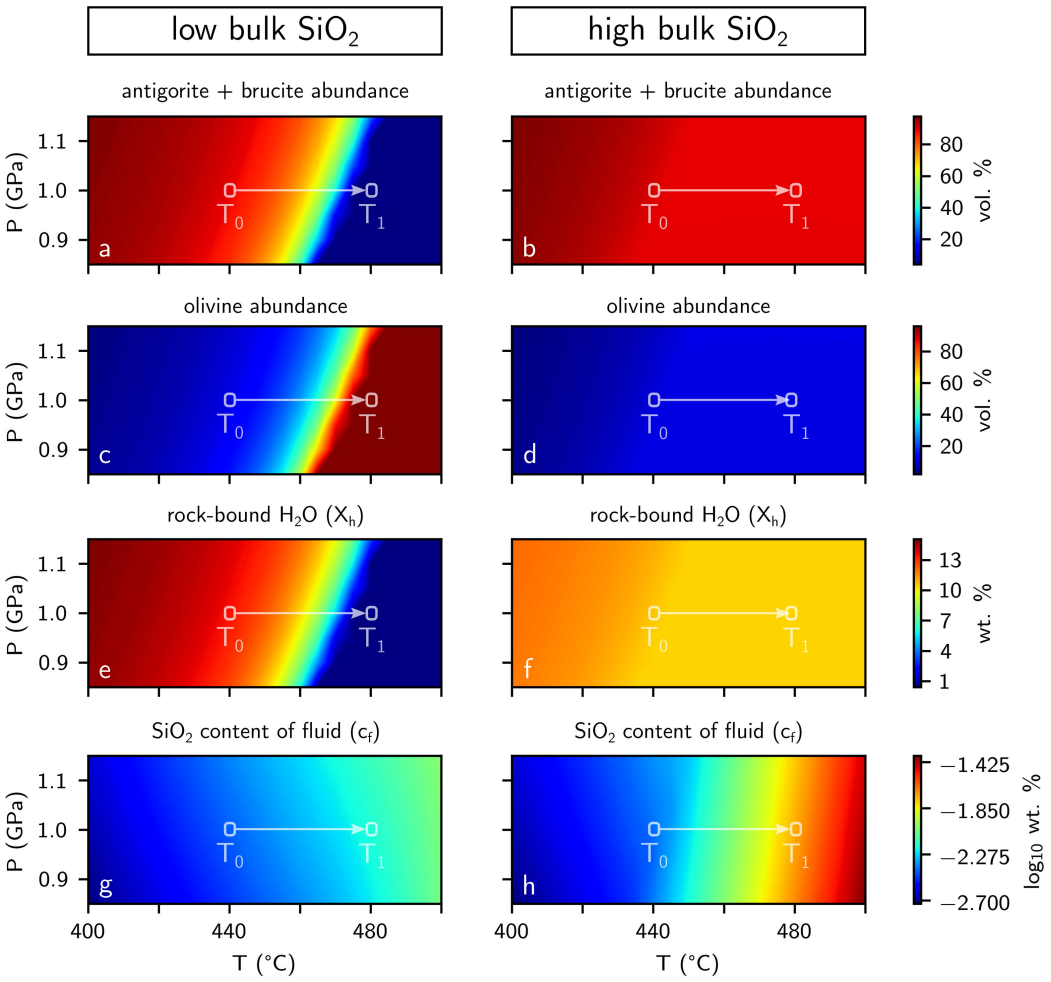

Figure 3. Effects of varying silica contents in a system with a high bulk iron content. A low silica content stabilizes more brucite which is only stable up to around 470 °C (a, b) and reacts with antigorite to form olivine (c, d). The sharp decrease in the brucite content in the low silica system between 450 °C and 475 °C leads to a stronger overall decrease in the amount of solid-bound H_2O in the low silica system (e, f) and thus to the liberation of more fluid. The fluid released from the low-silica system has a lower silica content compared to the fluid liberated from the high-silica system (g, h). The bulk composition of the low-silica system is used as source region in the numerical model (see fig. 5). The arrow connecting the white circles shows the temperature step in the numerical model from 440 °C (T_0) to 480 °C (T_1) at 1 GPa.

leads to a stronger decrease in the overall H_2O content of the solid (fig. 3e and f) and thus to the liberation of more fluid in the silica-poor system. The composition of the liberated fluid (fig. 3g and h) is very similar with respect to silica up to temperatures of around 450 °C. For higher temperatures, the fluid released from the low silica system also contains less dissolved silica than the fluid from the high silica system. A lower bulk silica content thus leads to i) a larger amount of liberated fluid during dehydration and ii) the generation of a low silica fluid at temperatures above ca. 450 °C.

These calculations show that a low silica content stabilizes higher brucite abundances at temperatures below ca. 475 °C. For higher temperatures, brucite breaks down and a fluid forms that is silica-poor compared to the fluid release from more antigorite-rich domains, i.e. the silica poor domains dehydrate stronger than the silica richer domains in this temperature range. The according local fluid overpressure then drives fluid flow of the silica-poor fluid into other areas of the porous network.

3.3 Equilibrium Relationship Between Fluid and Solid Silica Content

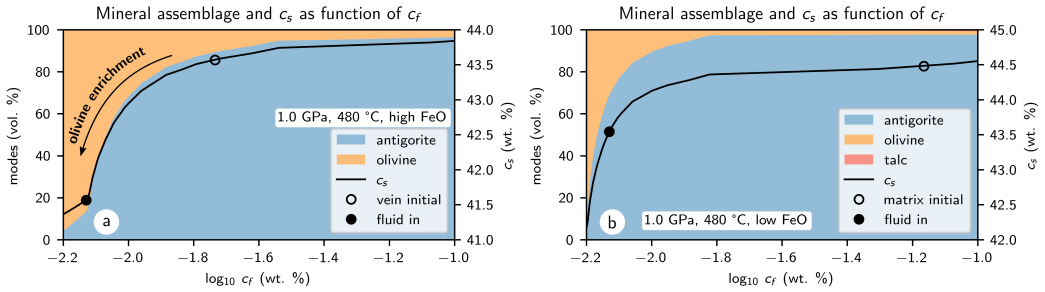

Figure 4. Equilibrium silica contents of fluid (c_f) and solid (c_s) in a system with high (a) and low (b) iron content at a fixed temperature of 480 °C (T_1) and a pressure of 1.0 GPa (P_f^0). The solid black line is the bulk silica content of the solid plotted against the fluid composition on the x axis. The colored areas in the background show the stable mineral assemblage in the rock for every value of c_s. Blue = antigorite, orange = olivine, red = talc. The open circles are plotted at the bulk composition of a typical hydrated serpentinite, the closed circles at a silica poor compostion (see also table 3). Lowering the fluid composition to reduced silica concentrations shifts the solid composition along the black curve towards the left, resulting in dehydration and olivine enrichment.

The equilibrium relationships between fluid composition, bulk silica content in the solid and the associated stable mineral assemblage are shown in figure 4. Figure 4a shows the result for a system with a high bulk iron, fig. 4b for a system with a low bulk iron content. In order to focus on the effect of changes in the bulk silica content only, the temperature and pressure are in both plots fixed to 480 °C and 1.0 GPa, respectively. Then, the silica content of the fluid (c_f) and the solid (c_s) change only as a function of the bulk silica content for the entire system and can be plotted against each other (solid black graph). The c_s graph shows that a decrease in the fluid silica content leads to a decrease in the solid silica content and vice versa. For every value of c_s, the stable mineral assemblage (in vol. %) is shown by the colored areas in the background. They show that a decrease in c_s leads to the breakdown of antigorite and the formation of olivine and thus to dehydration. In domains with a high iron content, this leads to olivine purification for fluid compositions between 0.016 ($10^{-1.8}$) and 0.008 ($10^{-2.1}$) wt. % of dissolved SiO_2 (fig. 4a), whereas lower iron contents stabilize higher amounts of antigorite in this range of fluid composition.

Changes in the fluid composition will shift the equilibrium of the surrounding (affected) rock along the c_s graph which triggers mineral reactions and thus changes in the mineral assemblage. Influx of a low silica fluid (closed circles) into a high silica domain (open circles) would therefore lower the c_s values of the affected rock from their initial values at the open circles towards lower values. In the high iron system (a), this may lead to the formation of an almost olivine-pure mineral assemblage.

4 Numerical Model

To investigate the dynamic effects of flow in a dehydrating serpentinite, we used a 2D numerical model that combines the findings of Plümper et al. (2017) with the effects of reactive transport by fluids carrying aqueous silica.

4.1 Setup

Observations from the Erro Tobbio meta-serpentinites show that the fluid is produced heterogeneously distributed in the rock and then pooled into larger veins (fig. 1). To simplify the problem, we set up three chemically distinct domains with varying bulk silica and bulk iron contents as shown in figure 5. The three domains represent i) a matrix with ii) a vein placed in its center and ii) a fluid source region from where fluid flows into the vein. Because we assume fluid flow from multiple fluid source regions into the vein, the composition of the fluid source region is set as a boundary condition to simulate a constant fluid influx from a region external but adjacent of our initial vein – wall rock assemblage.

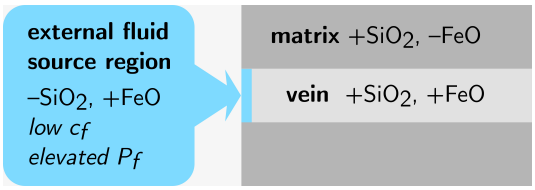

Figure 5. Conceptual sketch of the 2D model setup. A high silica domain with iron heterogeneities (grey areas) is connected to a fluid source region (blue), where elevated fluid pressure due to enhanced dehydration drives fluid flow of a low-silica fluid into the vein. The composition of the incoming fluid is defined by thermodynamic equilibrium with the solid of the source region.

4.2 Initial Conditions

Both matrix and vein have an initially high silica content, but the vein has also a high iron content whereas the matrix is low in iron (table 3). This is based on the findings of Plümper et al (2017) where iron was the main driver of the intrinsic chemical heterogeneities that resulted in a vein network formation. In the fluid source region at one end of the vein the silica content is lowered resulting in a high iron and a low silica content in this domain (see figure 5).

Initially, all three domains have zero background porosity ($\phi^0 = 0$) and a homogeneous fluid pressure ($P_f^0 = 1.0$ GPa, equal to ambient pressure) at an initial temperature (T_0) of 440 °C. This reflects a rather warm geotherm for a subduction zone (Syracuse et al., 2010) but since the dehydration reactions have very steep slopes in the P-T space, variations in pressure are less important.

Table 3. Initial bulk compositions in wt. % for the three domains in the numerical model. Vein and matrix composition have the same bulk SiO_2 content in moles.

	SiO_2	FeO	MgO	H_2O
vein	43.10	5.52	37.19	14.18
matrix	44.50	2.83	38.13	14.54
source region	41.48	5.68	38.25	14.59

To simulate dehydration during subduction, the temperature is instantaneously increased to 480 °C (fig. 1) to cross the 450 °C boundary at which the fluid composition of high- and low-silica systems start to vary significantly (fig. 3). Due to the heating dehydration starts in all three domains, however the extent of dehydration and the composition of the liberated fluid are different in all three domains as they depend on the bulk composition as in Plümper et al. (2017).

5 Results of the Numerical Model

The results of the numerical model are shown in figure 6. For every variable (figs. 6a-g) there is a column with three plots (subscript 1-3) displaying the initial conditions at temperature T_0 (1), after the temperature increase to T_1 (2) and after the influx of the low silica fluid (3).

5.1 Fluid Pressure

The initially homogeneous fluid pressure increases heterogeneously after the temperature increase, according to the local bulk composition that controls the extent of dehydration. The fluid source region shows the strongest dehydration and therefore also the highest fluid pressure. As the fluid pressure in the source region is kept constant, it also acts as a source region for fluid pressure. This local fluid overpressure drives fluid flow from the source region into the vein. As the silica content of the fluid released from the source region is the lowest of all three domains, fluid influx lowers the silica content of the fluid in the vein. Additionally, the silica content of the fluid is lowered by diffusion along the concentration gradient from the vein towards the source region. Although fluid flow and diffusion also occur between the fluid in the matrix and the vein, the extent is limited by the very low porosity in the matrix ($\phi = 0.0048$ in the matrix in contrast to $\phi = 0.085$ in the vein).

5.2 Porosity Evolution

The temperature increase leads to formation of porosity in the initially non-porous rock ($\phi^0 = 0$). At T_1 initial, porosity is highest in the source region (0.312), followed by the vein (0.085) and the matrix (0.0048). These calculated porosities reflect realistic values for subducted oceanic lithosphere at comparable P-T conditions (Katayama et al., 2012; Taetz et al., 2018). The increased porosity in the vein serves as pathway for the inflowing fluid from the source region and thus channelizes the fluid flow. Porosity then increases further by dehydration-related mineral reactions induced by the reactive fluid flow (fig. 3). Because dehydration, and thus porosity increase, is stronger in the vein than in the matrix, the fluid flow is even further channelized into the vein. Porosity increases also at the vein boundaries where the matrix dehydrates, leading to vein widening as reactive fluid flow continues.

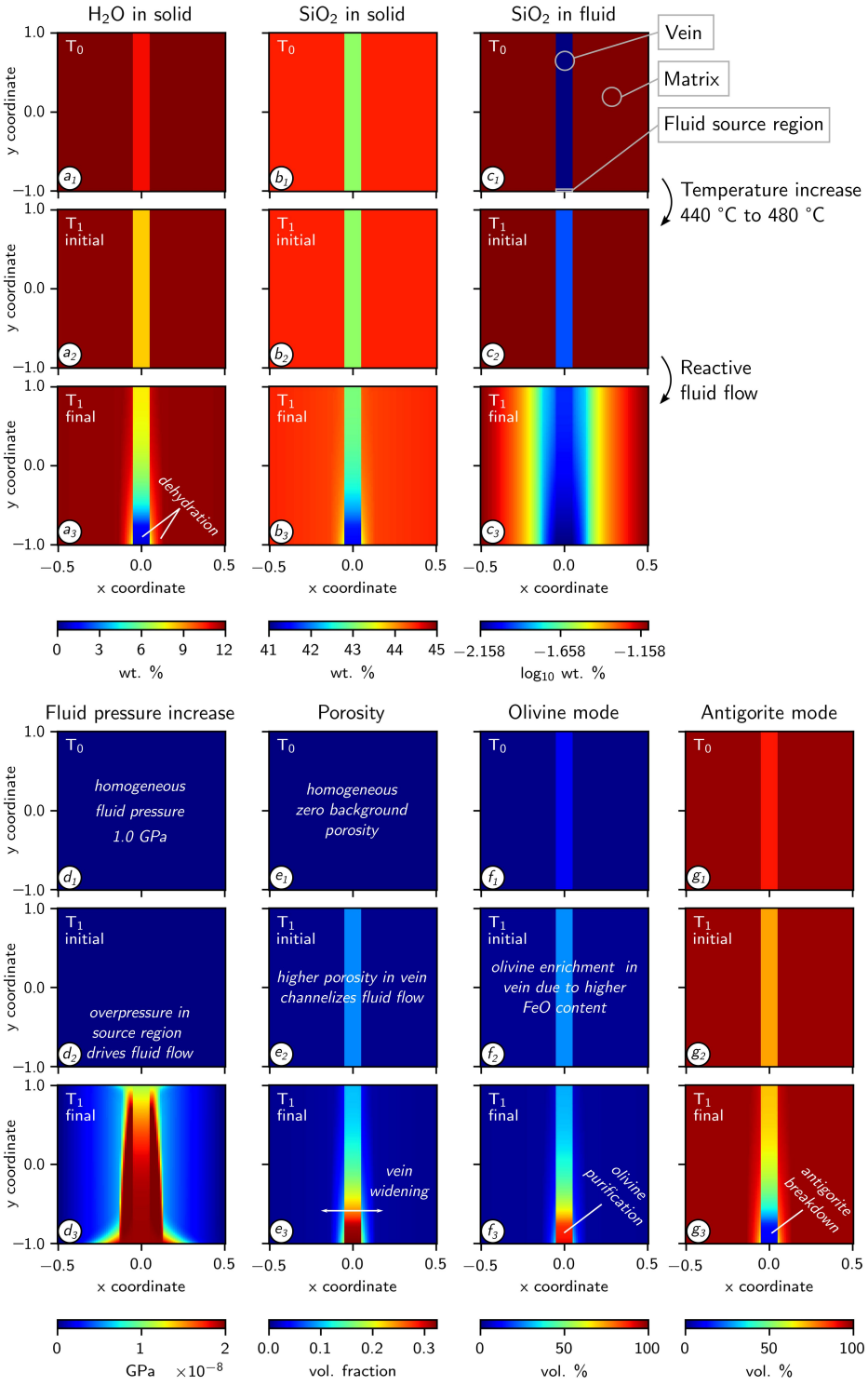

Figure 6. Results of the numerical model. For every variable (a-g) three plots are made at 1) the initial temperature T_0 (440 °C), 2) after the increase to T_1 (480 °C) and 3) after the influx of a low silica fluid. Influx of a low silica fluid from a fluid source region with low silica and high iron content into a vein with high silica and high iron content leads to dehydration and vein widening. The equilibrium within the vein is shifted towards olivine purification.

5.3 Olivine Enrichment and Antigorite Breakdown

The initial mineral assemblage in both matrix and vein is dominated by antigorite, although the vein initially contains more olivine due to the higher iron content. The influx of the low silica fluid shifts the equilibrium assemblage in the vein to almost pure olivine (fig. 3). Antigorite abundance in the vein decreases from 73.6 vol. % at T_1 initial to below 10 vol. % due to the reactive fluid flow. In contrast, the reactive fluid flow causes that antigorite contents in the matrix decrease from 97.6 vol. % at T_1 initial to 65.3 vol. % close to the boundary to vein. The olivine content in the vein reaches more than 90 vol. % directly at the boundary to the source region. Olivine enrichment in the matrix does not reach more than 34.7 vol. % in direct vicinity to the vein. The low iron content of the matrix of the vein wall rock stabilizes antigorite and prevents further dehydration.

6 Discussion

6.1 The Simplified FMSH System

In our model we simplified the chemical system compared to the model of Plümper et al. (2017) by excluding aluminum and calcium. The incorporation of aluminum (Tschermak's substitution) in antigorite, just like iron, lowers the temperature of the first antigorite breakdown (Padrón-Navarta et al., 2013). In addition, including aluminum also allows to account for the formation of chlorite which can retain H_2O in the solid for temperatures up to ca. 750 °C (e.g. Scambelluri et al., 2014). Calcium in serpentinites would be stored in either diopside (at higher pressures) or tremolite (at lower pressures). The abundance of these phases however is very limited in serpentinites because of their usually low calcium contents (e.g. bulk compositions of Li et al. (2004)).

The goal of this work was to study the effects of silica metasomatism and its first order effects on serpentinite dehydration after the formation of an initial fluid pathway, resulting from variations in the bulk rock chemistry. As both aluminum and iron have similar effect on the onset of dehydration, we chose the simplest chemical system necessary to describe a heterogeneously dehydrating serpentinite, while still having the effects of solid solution. Including only iron as component with a well-known effect on the onset of dehydration allows to better differentiate between porosity increase by the increase in temperature and by the reactive fluid flow. The simplified chemical system furthermore enabled us to use high-resolution lookup tables as only solid solutions between the magnesium and the iron endmembers need to be considered.

6.2 The Fluid Source Regions

In the numerical model the fluid source region has been assigned as a boundary condition that leads to a constant fluid influx into the vein. This source region does not necessarily represent a single spot in the rock but rather multiple volumes of rock that dehydrate and release a low silica fluid. We hypothesize that when the porosity and hence permeability in the porous media-like rock system is high enough, i.e. the percolation threshold is reached (e.g. Bloch et al., 2018), the fluid from these domains will channelize into larger veins as the one in our model.

The low silica and high iron content of the source regions stabilize significant amount of brucite at lower temperatures. In a natural serpentinite the source regions would therefore be brucite-rich domains that are distributed in the mantle section of interest. In fact, Klein et al. (2020) and Kempf et al. (2020) used the distribution of olivine-rich patches in the Zermatt ophiolite to infer to former brucite-rich spots. They also related the olivine-rich shear zones in the ophiolite to fluid pathways for the fluid released from the brucite-rich spots.

6.3 The Instantaneous Increase in Temperature

As no large temperature gradients are expected on the micro-scale we have taken a spatially homogeneous temperature throughout all domains. The instantaneous temperature increase in our model simulates the effect of subduction deeper down into the subduction zone, hence the descend into the hot mantle. In nature this temperature increase certainly happens more continuously. Smaller temperature steps would lead to a more continuous approximation of the dehydration process and a competition between the relaxation of the fluid pressure and the fluid chemistry gradients. Here the focus was on the process of fluid pressure relaxation and fluid composition evolution after a single step of heating. This allowed to study only the transient effects of reactive fluid flow in more detail. In order to simulate a more complete subduction zone dehydration process a more complex approach involving heat transport is needed. We chose the temperature range from 440 °C to 480 °C at which the reactive fluid flow becomes most likely important. Our calculations (fig. 3g and h) show that until a temperature of about 460 °C, the silica content of fluids derived from the high and the low silica domains are quite similar. Only at higher temperatures more silica is dissolved in the fluid the high silica system than in the low silica system and reactive fluid flow will be more effective.

6.4 Fe Dissolution in the Fluid

Although the dissolution of ferrous iron in aqueous fluids is very low (e.g. Charlou et al., 2002; Ding & Seyfried, 1992), Debret et al. (2016) show isotopic evidence for long-distance iron transport via subduction zone fluids. In a reduced serpentinite as used in our model, ferrous iron is mostly transported by forming sulfur and chlorine complexes (e.g. Chen et al., 2019). The amount of dissolved iron therefore also depends on the abundance of these elements in the serpentinite (Alt et al., 2013). A high concentration of iron in solution would also lead to iron exchange between the solid and the fluid and thus affect the iron content of the solid. Because of the large effect of the iron content on the dehydration reactions, the transport of iron in the fluid could amplify the effects of reactive fluid flow in addition to transport of aqueous silica.

6.5 Implications for Fluid Release in Subduction Zones

It has been shown in various studies that intraslab fluid flow and fluid escape from the slab is channelized and reactive, both to various degrees (Chen et al., 2019; Angiboust et al., 2014; Herms et al., 2012; John et al., 2012; Taetz et al., 2016). Our findings indicate that reactive fluid flow is able to transform an initially fine and small-scale high porosity structure into wider and larger vein systems that could also develop reaction halos. It reflects a first step towards a mechanistic understanding on how dehydration leads from the first stsage of chemistry-controlled local dehydration to the development of intra slab flow structures that are either highly channelized with only limited interaction with the wall rock (e.g. Breeding & Ague, 2002; Spandler et al., 2011), or highly channelized with significant reaction haloes surrounding the vein (e.g. Herms et al., 2012; Taetz et al., 2016; John et al., 2012), or even reflecting porosity wave-like high-permeability structures the are affecting rock volumes on cm to tens of meter scales without out necessarily having a fracture like vein structures (e.g. Piccoli et al., 2021; Chen et al., 2019).

7 Conclusions

Here, we have presented a reactive fluid flow model for transport of aqueous silica in a dehydrating serpentinite. We show how changes in the bulk silica and the bulk iron content affect the dehydration reaction of antigorite + brucite = olivine + fluid and the composition of this fluid with respect to silica. Domains with high bulk iron and sil-

ica contents dehydrate stronger and earlier than domains with higher silica and lower iron contents. The fluid released from these early dehydrating domains contains very low amounts of aqueous silica. Elevated fluid pressure in the stronger dehydrated domains will drive fluid flow of this low silica fluid into domains with higher silica contents where it causes dehydration and widening of existing veins by induced antigorite breakdown. In iron-rich domains the mineral assemblage can be shifted towards olivine purification whereas substantial amounts of antigorite remain stable in the iron-poor areas. This is in accordance with observations of olivine-rich veins in an antigorite-rich country rock as for example in the Erro-Tobbio meta-serpentinites.

Open Research

For our thermodynamic calculations we used MATLAB. The code and the thermodynamic data are available on request.

Acknowledgments

The Deutsche Forschungsgemeinschaft (DFG) financially supported this research through grant CRC 1114 'Scaling Cascades in Complex Systems', Project Number 235221301, Project (C09) – 'Dynamics of rock dehydration on multiple scales'. We also thank the mebers of the C09 project from the Weierstraß Institut (WIAS) in Berlin, M. Thomas, D. Peschka and A. Zafferi for their collaboration in this project and the fruitful discussions. The authors also thank M. Scambelluri for his collaboration and for helping us in the field.

References

Alt, J. C., Schwarzenbach, E. M., Früh-Green, G. L., Shanks, W. C., Bernasconi, S. M., Garrido, C. J., ... Marchesi, C. (2013). The role of serpentinites in cycling of carbon and sulfur: Seafloor serpentinization and subduction metamorphism. *Lithos*, *178*, 40–54. doi: 10.1016/j.lithos.2012.12.006

Angiboust, S., Pettke, T., De Hoog, J. C. M., Caron, B., & Oncken, O. (2014). Channelized Fluid Flow and Eclogite-facies Metasomatism along the Subduction Shear Zone. *J. Petrol.*, *55*(5), 883–916. doi: 10.1093/petrology/egu010

Beinlich, A., John, T., Vrijmoed, J. C., Tominaga, M., Magna, T., & Podladchikov, Y. Y. (2020). Instantaneous rock transformations in the deep crust driven by reactive fluid flow. *Nat. Geosci.*, *13*(4), 307–311. doi: 10.1038/s41561-020-0554-9

Bloch, W., John, T., Kummerow, J., Salazar, P., Krüger, O. S., & Shapiro, S. A. (2018). Watching Dehydration: Seismic Indication for Transient Fluid Pathways in the Oceanic Mantle of the Subducting Nazca Slab. *Geochem. Geophys. Geosyst.*, *19*(9), 3189–3207. doi: 10.1029/2018GC007703

Breeding, C. M., & Ague, J. J. (2002). Slab-derived fluids and quartz-vein formation in an accretionary prism, Otago Schist, New Zealand. *Geology*, *30*(6), 499–502. doi: 10.1130/0091-7613(2002)030⟨0499:SDFAQV⟩2.0.CO;2

Cerpa, N. G., Wada, I., & Wilson, C. R. (2017). Fluid migration in the mantle wedge: Influence of mineral grain size and mantle compaction. *Journal of Geophysical Research: Solid Earth*, *122*(8), 6247–6268. doi: 10.1002/2017JB014046

Charlou, J. L., Donval, J. P., Fouquet, Y., Jean-Baptiste, P., & Holm, N. (2002). Geochemistry of high H2 and CH4 vent fluids issuing from ultramafic rocks at the Rainbow hydrothermal field (36°14'N, MAR). *Chem. Geol.*, *191*(4), 345–359. doi: 10.1016/S0009-2541(02)00134-1

Chen, S., Hin, R. C., John, T., Brooker, R., Bryan, B., Niu, Y., & Elliott, T. (2019). Molybdenum systematics of subducted crust record reactive fluid flow from

underlying slab serpentine dehydration. *Nat Commun*, *10*(1), 4773. doi: 10.1038/s41467-019-12696-3

Clément, M., Padrón-Navarta, J. A., & Tommasi, A. (2020). Interplay between Fluid Extraction Mechanisms and Antigorite Dehydration Reactions (Val Malenco, Italian Alps). *J. Petrol.*, *60*(10), 1935–1962. doi: 10.1093/petrology/egz058

Debret, B., Millet, M.-A., Pons, M.-L., Bouilhol, P., Inglis, E., & Williams, H. (2016). Isotopic evidence for iron mobility during subduction. *Geology*, *44*(3), 215–218. doi: 10.1130/G37565.1

Ding, K., & Seyfried, W. E. (1992). Determination of Fe-Cl complexing in the low pressure supercritical region (NaCl fluid): Iron solubility constraints on pH of subseafloor hydrothermal fluids. *Geochim. Cosmochim. Acta*, *56*(10), 3681–3692. doi: 10.1016/0016-7037(92)90161-B

Fukumura, S., Okamoto, K., & Terabayashi, M. (2019). Metamorphic olivine after dehydration embrittlement in Serpentinite: Case study from the Shiraga Serpentinite mass in the Sanbagawa high P/T metamorphic belt, central Shikoku, Japan. *Isl. Arc*, *28*(2), e12293. doi: 10.1111/iar.12293

Groppo, C., & Compagnoni, R. (2007). Metamorphic Veins from the serpentinites of the Pieomonte Zone Western Alps: A Review. *Periodico di Mineralogia*, *76*(2-3), 127–153. doi: 10.2451/2007PM0021

Hacker, B. R., Peacock, S. M., Abers, G. A., & Holloway, S. D. (2003). Subduction factory 2. Are intermediate-depth earthquakes in subducting slabs linked to metamorphic dehydration reactions? *Journal of Geophysical Research: Solid Earth*, *108*(B1). doi: 10.1029/2001JB001129

Hermann, J., Müntener, O., & Scambelluri, M. (2000). The importance of serpentinite mylonites for subduction and exhumation of oceanic crust. *Tectonophysics*, *327*(3), 225–238. doi: 10.1016/S0040-1951(00)00171-2

Herms, P., John, T., Bakker, R. J., & Schenk, V. (2012). Evidence for channelized external fluid flow and element transfer in subducting slabs (Raspas Complex, Ecuador). *Chem. Geol.*, *310-311*, 79–96. doi: 10.1016/j.chemgeo.2012.03.023

Holland, T., & Powell, R. (1991). A Compensated-Redlich-Kwong (CORK) equation for volumes and fugacities of CO2 and H2O in the range 1 bar to 50 kbar and 100–1600°C. *Contrib. Mineral. Petrol.*, *109*(2), 265–273. doi: 10.1007/BF00306484

Holland, T. J. B., & Powell, R. (1998). An internally consistent thermodynamic data set for phases of petrological interest. *J. Metamorph. Geol.*, *16*(3), 309–343. doi: 10.1111/j.1525-1314.1998.00140.x

John, T., Gussone, N., Podladchikov, Y. Y., Bebout, G. E., Dohmen, R., Halama, R., ... Seitz, H.-M. (2012). Volcanic arcs fed by rapid pulsed fluid flow through subducting slabs. *Nat. Geosci.*, *5*(7), 489–492. doi: 10.1038/ngeo1482

John, T., Klemd, R., Gao, J., & Garbe-Schönberg, C.-D. (2008). Trace-element mobilization in slabs due to non steady-state fluid–rock interaction: Constraints from an eclogite-facies transport vein in blueschist (Tianshan, China). *Lithos*, *103*(1), 1–24. doi: 10.1016/j.lithos.2007.09.005

Jung, H., Green II, H. W., & Dobrzhinetskaya, L. F. (2004). Intermediate-depth earthquake faulting by dehydration embrittlement with negative volume change. *Nature*, *428*(6982), 545–549. doi: 10.1038/nature02412

Katayama, I., Terada, T., Okazaki, K., & Tanikawa, W. (2012). Episodic tremor and slow slip potentially linked to permeability contrasts at the Moho. *Nat. Geosci.*, *5*(10), 731–734. doi: 10.1038/ngeo1559

Kempf, E. D., Hermann, J., Reusser, E., Baumgartner, L. P., & Lanari, P. (2020). The role of the antigorite + brucite to olivine reaction in subducted serpentinites (Zermatt, Switzerland). *Swiss J Geosci*, *113*(1), 16.

Klein, F., Humphris, S. E., & Bach, W. (2020). Brucite formation and dissolution

in oceanic serpentinite. *Geochemical Perspectives Letters*, 1–5. doi: 10.7185/geochemlet.2035

Li, X.-P., Rahn, M., & Bucher, K. (2004). Serpentinites of the Zermatt-Saas ophiolite complex and their texture evolution. *J. Metamorph. Geol.*, *22*(3), 159–177. doi: 10.1111/j.1525-1314.2004.00503.x

López Sánchez-Vizcaíno, V., Gómez-Pugnaire, M. T., Garrido, C. J., Padrón-Navarta, J. A., & Mellini, M. (2009). Breakdown mechanisms of titanclinohumite in antigorite serpentinite (Cerro del Almirez massif, S. Spain): A petrological and TEM study. *Lithos*, *107*(3), 216–226. doi: 10.1016/j.lithos.2008.10.008

López Sánchez-Vizcaíno, V., Trommsdorff, V., Gómez-Pugnaire, M. T., Garrido, C. J., Müntener, O., & Connolly, J. A. D. (2005). Petrology of titanian clinohumite and olivine at the high-pressure breakdown of antigorite serpentinite to chlorite harzburgite (Almirez Massif, S. Spain). *Contrib. Mineral. Petrol.*, *149*(6), 627–646. doi: 10.1007/s00410-005-0678-3

Magott, R., Fabbri, O., & Fournier, M. (2020). Seismically-induced serpentine dehydration as a possible mechanism of water release in subduction zones. Insights from the Alpine Corsica pseudotachylyte-bearing Monte Maggiore ophiolitic unit. *Lithos*, *362-363*, 105474. doi: 10.1016/j.lithos.2020.105474

Malvoisin, B., Podladchikov, Y. Y., & Vrijmoed, J. C. (2015). Coupling changes in densities and porosity to fluid pressure variations in reactive porous fluid flow: Local thermodynamic equilibrium. *Geochem. Geophys. Geosyst.*, *16*(12), 4362–4387. doi: 10.1002/2015GC006019

Manning, C. E. (2004). The chemistry of subduction-zone fluids. *Earth Planet. Sci. Lett.*, *223*(1), 1–16. doi: 10.1016/j.epsl.2004.04.030

Mazza, S. E., Stracke, A., Gill, J. B., Kimura, J.-I., & Kleine, T. (2020). Tracing dehydration and melting of the subducted slab with tungsten isotopes in arc lavas. *Earth Planet. Sci. Lett.*, *530*, 115942. doi: 10.1016/j.epsl.2019.115942

McGary, R. S., Evans, R. L., Wannamaker, P. E., Elsenbeck, J., & Rondenay, S. (2014). Pathway from subducting slab to surface for melt and fluids beneath Mount Rainier. *Nature*, *511*(7509), 338–340. doi: 10.1038/nature13493

Merkulova, M., Muñoz, M., Vidal, O., & Brunet, F. (2016). Role of iron content on serpentinite dehydration depth in subduction zones: Experiments and thermodynamic modeling. *Lithos*, *264*, 441–452. doi: 10.1016/j.lithos.2016.09.007

Miller, S. A., van der Zee, W., Olgaard, D. L., & Connolly, J. A. D. (2003). A fluid-pressure feedback model of dehydration reactions: experiments, modelling, and application to subduction zones. *Tectonophysics*, *370*(1), 241–251. doi: 10.1016/S0040-1951(03)00189-6

Moreno, M., Haberland, C., Oncken, O., Rietbrock, A., Angiboust, S., & Heidbach, O. (2014). Locking of the Chile subduction zone controlled by fluid pressure before the 2010 earthquake. *Nat. Geosci.*, *7*(4), 292–296. doi: 10.1038/ngeo2102

Padrón-Navarta, J. A., Sánchez-Vizcaíno, V. L., Hermann, J., Connolly, J. A. D., Garrido, C. J., Gómez-Pugnaire, M. T., & Marchesi, C. (2013). Tschermak's substitution in antigorite and consequences for phase relations and water liberation in high-grade serpentinites. *Lithos*, *178*, 186–196. doi: 10.1016/j.lithos.2013.02.001

Padrón-Navarta, J. A., Tommasi, A., Garrido, C. J., Sánchez-Vizcaíno, V. L., Gómez-Pugnaire, M. T., Jabaloy, A., & Vauchez, A. (2010). Fluid transfer into the wedge controlled by high-pressure hydrofracturing in the cold top-slab mantle. *Earth Planet. Sci. Lett.*, *297*(1), 271–286. doi: 10.1016/j.epsl.2010.06.029

Piccoli, F., Ague, J. J., Chu, X., Tian, M., & Vitale Brovarone, A. (2021). Field-Based Evidence for Intra-Slab High-Permeability Channel Formation at Eclogite-Facies Conditions During Subduction. *Geochem. Geophys. Geosyst.*,

22(3), e2020GC009520. doi: 10.1029/2020GC009520

Plümper, O., John, T., Podladchikov, Y. Y., Vrijmoed, J. C., & Scambelluri, M. (2017). Fluid escape from subduction zones controlled by channel-forming reactive porosity. *Nat. Geosci.*, *10*(2), 150–156. doi: 10.1038/ngeo2865

Powell, R., & Holland, T. (1999). Relating formulations of the thermodynamics of mineral solid solutions; activity modeling of pyroxenes, amphiboles, and micas. *Am. Mineral.*, *84*(1-2), 1-14. doi: 10.2138/am-1999-1-201

Rüpke, L., Morgan, J. P., Hort, M., & Connolly, J. A. D. (2004). Serpentine and the subduction zone water cycle. *Earth Planet. Sci. Lett.*, *223*(1), 17–34. doi: 10.1016/j.epsl.2004.04.018

Scambelluri, M., Müntener, O., Hermann, J., Piccardo, G. B., & Trommsdorff, V. (1995). Subduction of water into the mantle: History of an Alpine peridotite. *Geology*, *23*(5), 459–462. doi: 10.1130/0091-7613(1995)023⟨0459:SOWITM⟩2.3.CO;2

Scambelluri, M., Pettke, T., Rampone, E., Godard, M., & Reusser, E. (2014). Petrology and Trace Element Budgets of High-pressure Peridotites Indicate Subduction Dehydration of Serpentinized Mantle (Cima di Gagnone, Central Alps, Switzerland). *J. Petrol.*, *55*(3), 459–498. doi: 10.1093/petrology/egt068

Scambelluri, M., Strating, E. H. H., Piccardo, G. B., Vissers, R. L. M., & Rampone, E. (1991). Alpine olivine- and titanian clinohumite-bearing assemblages in the Erro-Tobbio peridotite (Voltri Massif, NW Italy). *J. Metamorph. Geol.*, *9*(1), 79–91. doi: 10.1111/j.1525-1314.1991.tb00505.x

Schmidt, M. W., & Poli, S. (1998). Experimentally based water budgets for dehydrating slabs and consequences for arc magma generation. *Earth Planet. Sci. Lett.*, *163*(1), 361–379. doi: 10.1016/S0012-821X(98)00142-3

Skarbek, R. M., & Rempel, A. W. (2016). Dehydration-induced porosity waves and episodic tremor and slip. *Geochem. Geophys. Geosyst.*, *17*(2), 442–469. doi: 10.1002/2015GC006155

Spandler, C., Pettke, T., & Rubatto, D. (2011). Internal and External Fluid Sources for Eclogite-facies Veins in the Monviso Meta-ophiolite, Western Alps: Implications for Fluid Flow in Subduction Zones. *J. Petrol.*, *52*(6), 1207–1236. doi: 10.1093/petrology/egr025

Spear, F. S. (1993). *Metamorphic Phase Equilibria and Pressure-Temperature-Time Paths*. Mineralogical Society of America.

Syracuse, E. M., van Keken, P. E., & Abers, G. A. (2010). The global range of subduction zone thermal models. *Phys. Earth Planet. In.*, *183*(1), 73–90. doi: 10.1016/j.pepi.2010.02.004

Taetz, S., John, T., Bröcker, M., & Spandler, C. (2016). Fluid–rock interaction and evolution of a high-pressure/low-temperature vein system in eclogite from New Caledonia: insights into intraslab fluid flow processes. *Contrib. Mineral. Petrol.*, *171*(11), 90. doi: 10.1007/s00410-016-1295-z

Taetz, S., John, T., Bröcker, M., Spandler, C., & Stracke, A. (2018). Fast intraslab fluid-flow events linked to pulses of high pore fluid pressure at the subducted plate interface. *Earth Planet. Sci. Lett.*, *482*, 33–43. doi: 10.1016/j.epsl.2017.10.044

Ulmer, P., & Trommsdorff, V. (1995). Serpentine stability to mantle depths and subduction-related magmatism. *Science*, *268*(5212), 858–861. doi: 10.1126/science.268.5212.858

van Keken, P. E., Hacker, B. R., Syracuse, E. M., & Abers, G. A. (2011). Subduction factory: 4. Depth-dependent flux of H2O from subducting slabs worldwide. *Journal of Geophysical Research: Solid Earth*, *116*(B1). doi: 10.1029/2010JB007922

Vrijmoed, J. C., & Podladchikov, Y. Y. (2015). Thermodynamic equilibrium at heterogeneous pressure. *Contrib. Mineral. Petrol.*, *170*(1), 10. doi: 10.1007/s00410-015-1156-1

Wilson, C. R., Spiegelman, M., van Keken, P. E., & Hacker, B. R. (2014). Fluid flow in subduction zones: The role of solid rheology and compaction pressure. *Earth Planet. Sci. Lett.*, *401*, 261–274. doi: 10.1016/j.epsl.2014.05.052